

CFD Analysis of a Minimum-Length Nozzle Designed with the Method of Characteristics

Enes Çelik (B.Sc. Student)

September 11, 2025

Abstract

This study designs and verifies a *minimum-length* (ML) supersonic nozzle using the Method of Characteristics (MOC) and computational fluid dynamics (CFD). The target case is air ($\gamma = 1.4$) with a design exit Mach number $M_e = 3.05$ and geometric constraints $D_{in} = 2.0 \times 10^0$ m and $D_e = 1.0 \times 10^0$ m. The wall contour is generated by a centered-fan MOC construction in which the throat wall turn is $\nu(M_e)/2$. The computed flow on structured multi-block meshes agrees with isentropic theory and the characteristic design. Exit-plane Mach is uniform and the solution is mesh-independent within typical engineering tolerances. The full workflow—parameters, formulas, marching rules, and solver settings—is included to enable reproducibility.

Nomenclature

Gas/thermo

γ	Ratio of specific heats (-)
R	Specific gas constant ($\text{J kg}^{-1} \text{K}^{-1}$)
$a = \sqrt{\gamma p/\rho}$	Speed of sound (m s^{-1})
c_p	Specific heat at constant pressure ($\text{J kg}^{-1} \text{K}^{-1}$)

Flow variables

ρ	Density (kg m^{-3})
u, v	Cartesian velocity components (m s^{-1})
$V = \sqrt{u^2 + v^2}$	Velocity magnitude (m s^{-1})
h, E	Static enthalpy and total energy per unit mass (J kg^{-1})
p, p_0	Static and stagnation pressure (Pa)
T, T_0	Static and stagnation temperature (K)
\dot{m}	Mass flow rate (kg s^{-1})
G^*	Choked mass flux ($\text{kg m}^{-2} \text{s}^{-1}$)

Kinematics/MOC

M	Mach number (-)
$\nu(M)$	Prandtl–Meyer function (rad or $^\circ$)
θ	Flow turning angle from the x -axis (rad or $^\circ$)
μ_M	Mach angle, $\mu_M = \arcsin(1/M)$ (rad or $^\circ$)
$K^+ = \theta + \nu$	Riemann invariant (constant along C^-)
$K^- = \theta - \nu$	Riemann invariant (constant along C^+)
C^+, C^-	Characteristic families with slopes $\tan(\theta \pm \mu_M)$
Φ	Velocity potential, $u = \Phi_x, v = \Phi_y$
θ_w	Local wall angle; $\theta_{w,\max}$ its maximum (ML design)

Geometry/scaling

x, y	Axial and radial coordinates (m)
r	Local radius (m)
A, A^*, A_e	Local, throat and exit area (m^2)
R_i, R_t, R_e	Inlet, throat and exit radius (m)
D_{in}, D_*, D_e	Inlet, throat and exit diameter (m)
L_c, L_{div}	Converging- and diverging-section length (m)
s	Normalized arc/axial parameter in contraction, $s \in [0, 1]$ (-)
p_b, p_e	Back (outlet) and exit static pressure (Pa)

CFD (transport/closure)

μ	Laminar (molecular) dynamic viscosity ($\text{kg m}^{-1} \text{s}^{-1}$)
μ_t	Eddy (turbulent) viscosity ($\text{kg m}^{-1} \text{s}^{-1}$)
λ, λ_t	Laminar and turbulent thermal conductivity ($\text{W m}^{-1} \text{K}^{-1}$)
Pr, Pr_t	Laminar and turbulent Prandtl numbers (-)
τ^{eff}	Effective viscous stress tensor (Pa)
\mathbf{q}^{eff}	Effective heat flux (W m^{-2})
k, ω	Turbulent kinetic energy and specific dissipation (SST model)
S	Strain-rate magnitude used in SST limiter (s^{-1})
F_1, F_2	SST blending functions (-)

1 Introduction

Supersonic nozzles accelerate gas from sonic to supersonic speeds by expanding a high-enthalpy gas through a converging–diverging passage. For a specified exit Mach number, a *minimum-length* (ML) contour achieves the shortest nozzle that still produces a uniform, shock-free exit flow at the design condition. Such contours are attractive for weight- and volume-limited systems and as baselines for later viscous and thermal optimization.

The Method of Characteristics (MOC) provides a direct way to construct ML profiles. In a steady, inviscid, adiabatic, planar flow of a calorically perfect gas, the governing equations are hyperbolic for $M > 1$ and admit two families of characteristic lines, C^+ and C^- . Along these lines the combinations $\theta \pm \nu(M)$ remain constant, where θ is the local flow angle and ν is the Prandtl–Meyer function. An ML nozzle is obtained by launching a centered expansion fan from the throat with a maximum wall turn of $\nu(M_e)/2$, reflecting the waves from the centerline, and terminating the contour where the final C^+ meets the wall at zero angle. This procedure gives a uniform exit flow oriented normally to the exit plane.

In this work we target air ($\gamma = 1.4$) with $M_e = 3.05$ and $D_{in} = 2.0 \times 10^0$ m, $D_e = 1.0 \times 10^0$ m. The characteristic net is discretized to generate wall points which are then smoothed by a C^1 spline for manufacturability. The contour is evaluated using a finite-volume solver (SU2) on successively refined structured meshes. We quantify exit Mach uniformity, wall pressure against isentropic theory, and mass-flow consistency with choked predictions, showing that the characteristic design meets its objective.

2 Governing Equations and Reduction to the Full–Potential Form

2.1 Assumptions

Steady, inviscid, adiabatic, two-dimensional, irrotational, calorically perfect gas with $a^2 = (\partial p / \partial \rho)_s = \gamma p / \rho$.

2.2 Starting equations

Continuity

$$\frac{\partial(\rho u)}{\partial x} + \frac{\partial(\rho v)}{\partial y} = 0. \quad (1)$$

Euler momentum (steady, inviscid)

$$\begin{aligned} u \frac{\partial u}{\partial x} + v \frac{\partial u}{\partial y} + \frac{1}{\rho} \frac{\partial p}{\partial x} &= 0, \\ u \frac{\partial v}{\partial x} + v \frac{\partial v}{\partial y} + \frac{1}{\rho} \frac{\partial p}{\partial y} &= 0, \end{aligned} \quad (2)$$

Irrotationality

$$\frac{\partial v}{\partial x} - \frac{\partial u}{\partial y} = 0. \quad (3)$$

2.3 Bernoulli + isentropic link

Steady adiabatic flow has

$$h + \frac{V^2}{2} = h_0 = \text{const}, \quad V = \sqrt{u^2 + v^2}. \quad (4)$$

Differentiating and using $dh = dp/\rho$ (isentropic):

$$\frac{1}{\rho} dp + V dV = 0 \implies \nabla p = -\rho V \nabla V. \quad (5)$$

With $dp = a^2 d\rho$,

$$a^2 \nabla \rho = \nabla p = -\rho V \nabla V \implies \nabla \rho = -\frac{\rho V}{a^2} \nabla V. \quad (6)$$

Because $V = \sqrt{u^2 + v^2}$,

$$\begin{aligned} \frac{\partial V}{\partial x} &= \frac{u \frac{\partial u}{\partial x} + v \frac{\partial v}{\partial x}}{V}, \\ \frac{\partial V}{\partial y} &= \frac{u \frac{\partial u}{\partial y} + v \frac{\partial v}{\partial y}}{V}. \end{aligned} \quad (7)$$

Insert (7) into (6) to get

$$\begin{aligned} \frac{\partial \rho}{\partial x} &= -\frac{\rho}{a^2} \left(u \frac{\partial u}{\partial x} + v \frac{\partial v}{\partial x} \right), \\ \frac{\partial \rho}{\partial y} &= -\frac{\rho}{a^2} \left(u \frac{\partial u}{\partial y} + v \frac{\partial v}{\partial y} \right). \end{aligned} \quad (8)$$

2.4 Eliminate density gradients from continuity

Expand (1) and divide by ρ :

$$\frac{\partial u}{\partial x} + \frac{\partial v}{\partial y} + \frac{u}{\rho} \frac{\partial \rho}{\partial x} + \frac{v}{\rho} \frac{\partial \rho}{\partial y} = 0. \quad (9)$$

Use (8) in (9):

$$\begin{aligned} \frac{\partial u}{\partial x} + \frac{\partial v}{\partial y} - \frac{u}{a^2} \left(u \frac{\partial u}{\partial x} + v \frac{\partial v}{\partial x} \right) - \frac{v}{a^2} \left(u \frac{\partial u}{\partial y} + v \frac{\partial v}{\partial y} \right) &= 0, \\ \implies \left(1 - \frac{u^2}{a^2} \right) \frac{\partial u}{\partial x} + \left(1 - \frac{v^2}{a^2} \right) \frac{\partial v}{\partial y} - \frac{uv}{a^2} \left(\frac{\partial v}{\partial x} + \frac{\partial u}{\partial y} \right) &= 0. \end{aligned} \quad (10)$$

Invoke irrotationality (3) ($\partial v / \partial x = \partial u / \partial y$) to obtain the **velocity form of the 2D full-potential equation**:

$$\boxed{\left(1 - \frac{u^2}{a^2} \right) \frac{\partial u}{\partial x} + \left(1 - \frac{v^2}{a^2} \right) \frac{\partial v}{\partial y} - \frac{2uv}{a^2} \frac{\partial u}{\partial y} = 0} \quad (11)$$

2.5 Equivalent potential form

For irrotational flow, set $u = \Phi_x$, $v = \Phi_y$; then (11) becomes the familiar **full-potential equation**:

$$\boxed{\left(1 - \frac{u^2}{a^2} \right) \Phi_{xx} - \frac{2uv}{a^2} \Phi_{xy} + \left(1 - \frac{v^2}{a^2} \right) \Phi_{yy} = 0} \quad (12)$$

with $u = \Phi_x$, $v = \Phi_y$. It is hyperbolic for $M > 1$, parabolic for $M = 1$, and elliptic for $M < 1$.

3 Method of Characteristics (MOC)

3.1 Philosophy: why characteristics exist

Consider a steady 2D flow. If we advance a variable u from (i, j) to $(i + 1, j)$ in x and neglect higher-order terms,

$$u_{i+1,j} = u_{i,j} + \left(\frac{\partial u}{\partial x} \right)_{i,j} \Delta x + \dots \quad (13)$$

The derivative $\partial u / \partial x$ comes from the governing equations. For a two-dimensional *irrotational* compressible flow the steady *full potential* equation (nonlinear) is

$$\left(1 - \frac{u^2}{a^2} \right) \frac{\partial u}{\partial x} + \left(1 - \frac{v^2}{a^2} \right) \frac{\partial v}{\partial y} - \frac{2uv}{a^2} \frac{\partial u}{\partial y} = 0, \quad (14)$$

which yields, solved for $\partial u / \partial x$,

$$\frac{\partial u}{\partial x} = \frac{\frac{2uv}{a^2} \frac{\partial u}{\partial y} - \left(1 - \frac{v^2}{a^2} \right) \frac{\partial v}{\partial y}}{\left(1 - \frac{u^2}{a^2} \right)}. \quad (15)$$

When the denominator of (15) vanishes ($u = a$; i.e. the component normal to a vertical line is sonic), $\partial u / \partial x$ becomes indeterminate, and the directions along which such indeterminacy occurs are called *characteristic lines* (Mach lines). Figure 1 illustrates the Mach angle μ .

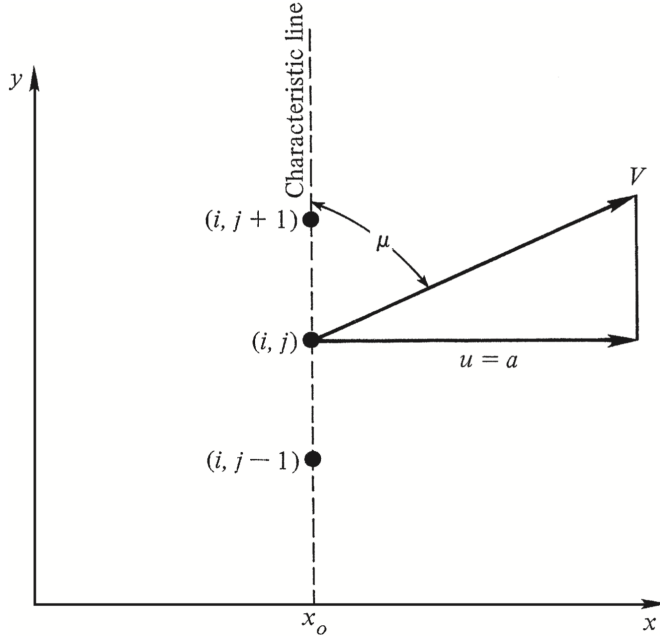


Figure 1: Characteristic direction at a sonic line and Mach angle μ .

Three-step philosophy (summary).

1. Identify lines in the xy -plane along which the field variables are continuous but their derivatives may be indeterminate: the *characteristic lines*.
2. Combine the PDEs to obtain ODEs that hold *only* along characteristics: the *compatibility equations*.

3. March the solution along the characteristics using the compatibility equations (the “unit processes”).

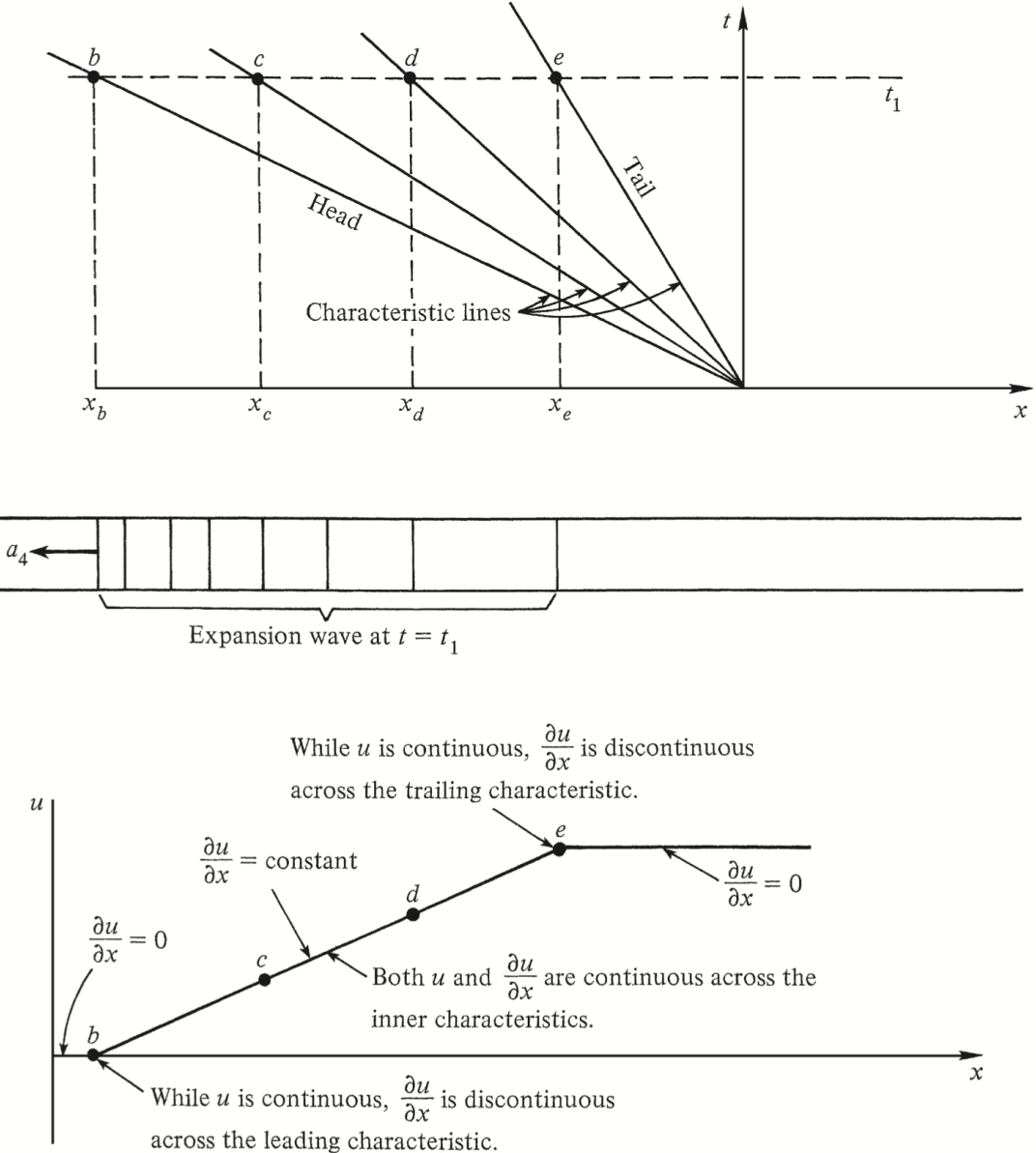


Figure 2: Unsteady 1D analogy: expansion fan and characteristic lines. While u is continuous, $\partial u / \partial x$ can jump across the leading/trailing characteristics.

3.2 Determination of the characteristic lines (2D, irrotational)

Let Φ be the velocity potential with $u = \Phi_x$, $v = \Phi_y$. The full-potential equation in terms of Φ is

$$\left(1 - \frac{\Phi_x^2}{a^2}\right)\Phi_{xx} + \left(1 - \frac{\Phi_y^2}{a^2}\right)\Phi_{yy} - \frac{2\Phi_x\Phi_y}{a^2}\Phi_{xy} = 0. \quad (16)$$

Since $u = \Phi_x$, $v = \Phi_y$, the differentials are

$$\begin{aligned} d(\Phi_x) &= \Phi_{xx} dx + \Phi_{xy} dy, \\ d(\Phi_y) &= \Phi_{yx} dx + \Phi_{yy} dy. \end{aligned} \quad (17)$$

Treat (16) and (17) as three linear algebraic equations in the unknowns $X = \Phi_{xx}$, $Y = \Phi_{xy}$, $Z = \Phi_{yy}$. Using Cramer's rule, the mixed derivative is

$$\Phi_{xy} = \frac{N}{D} = \frac{\begin{vmatrix} 1 - \frac{u^2}{a^2} & 0 & 1 - \frac{v^2}{a^2} \\ \frac{du}{dx} & 0 & 0 \\ 0 & \frac{dv}{dy} & \frac{dy}{dx} \end{vmatrix}}{\begin{vmatrix} 1 - \frac{u^2}{a^2} & -\frac{2uv}{a^2} & 1 - \frac{v^2}{a^2} \\ \frac{du}{dx} & \frac{dy}{dx} & 0 \\ 0 & \frac{dx}{dy} & \frac{dy}{dx} \end{vmatrix}}. \quad (18)$$

The indeterminacy occurs where $D = 0$; these directions in the xy -plane are the characteristic lines. Setting $D = 0$ gives

$$\left(1 - \frac{u^2}{a^2}\right)(dy)^2 + \frac{2uv}{a^2} dx dy + \left(1 - \frac{v^2}{a^2}\right)(dx)^2 = 0, \quad (19)$$

or, as a quadratic for the slope,

$$\left(\frac{dy}{dx}\right)_{\text{char}} = \frac{-\frac{2uv}{a^2} \pm \sqrt{\left(\frac{2uv}{a^2}\right)^2 - 4\left(1 - \frac{u^2}{a^2}\right)\left(1 - \frac{v^2}{a^2}\right)}}{2\left(1 - \frac{u^2}{a^2}\right)}. \quad (20)$$

The term under the root simplifies to

$$\frac{u^2 + v^2}{a^2} - 1 = \frac{V^2}{a^2} - 1 = M^2 - 1,$$

so for $M > 1$ there are two real characteristic directions through each point (hyperbolic).

Streamline geometry and the Mach angle (Fig. 11.7)

At point A in Fig. 3, let $u = V \cos \theta$ and $v = V \sin \theta$; then (20) becomes

$$\left(\frac{dy}{dx}\right)_{\text{char}} = \frac{-\frac{V^2}{a^2} \sin \theta \cos \theta \pm \sqrt{M^2 - 1}}{1 - \frac{V^2}{a^2} \cos^2 \theta}. \quad (21)$$

Using $\sin \mu = 1/M$ (hence $\tan \mu = 1/\sqrt{M^2 - 1}$ and $1/\tan \mu = \sqrt{M^2 - 1}$), (21) can be written as

$$\left(\frac{dy}{dx}\right)_{\text{char}} = \frac{-\frac{\cos \theta \sin \theta}{\sin^2 \mu} \pm \frac{1}{\tan \mu}}{1 - \frac{\cos^2 \theta}{\sin^2 \mu}}. \quad (22)$$

After straightforward trigonometric manipulation (multiply top and bottom by $\sin^2 \mu$ and use sum/difference formulas), this reduces to the compact and standard result

$$\boxed{\left.\frac{dy}{dx}\right|_{\text{char}} = \tan(\theta \mp \mu)} \iff \begin{cases} C^- : \frac{dy}{dx} = \tan(\theta - \mu), \\ C^+ : \frac{dy}{dx} = \tan(\theta + \mu). \end{cases} \quad (23)$$

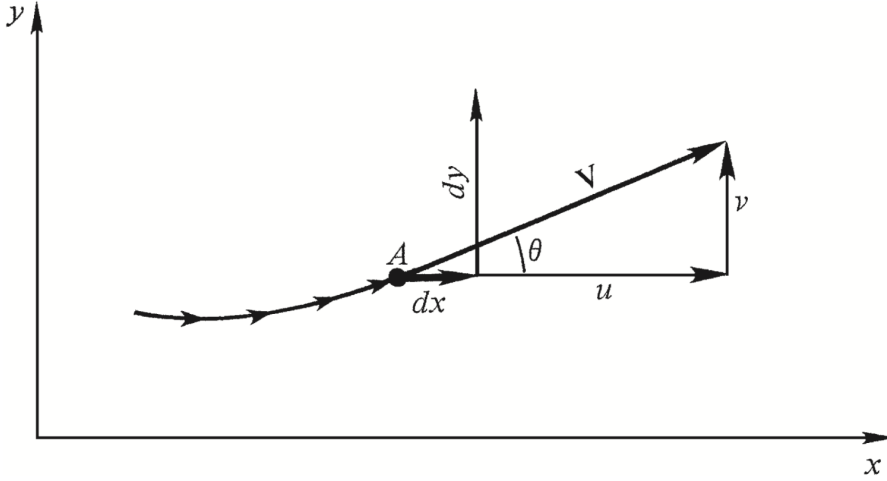


Figure 3: Streamline geometry at point A : $u = V \cos \theta$, $v = V \sin \theta$.

3.3 Compatibility (Riemann) relations

To obtain relations for the *variation* of the flow along characteristics, set the *numerator* in (18) to zero ($N = 0$). This gives

$$\left(1 - \frac{u^2}{a^2}\right) du dy + \left(1 - \frac{v^2}{a^2}\right) dv dx = 0, \quad \Rightarrow \quad \frac{dv}{du} = - \frac{\left(1 - \frac{u^2}{a^2}\right) \frac{dy}{dx}}{1 - \frac{v^2}{a^2}}. \quad (24)$$

Restricting attention to *characteristic* directions by substituting (23) (or (21)) into (24), one obtains after algebra

$$\frac{dv}{du} = \frac{\frac{uv}{a^2} \mp \sqrt{\frac{u^2 + v^2}{a^2} - 1}}{1 - \frac{v^2}{a^2}}, \quad (25)$$

where the upper (lower) sign applies on C^- (C^+). Using $u = V \cos \theta$, $v = V \sin \theta$,

$$\frac{d(V \sin \theta)}{d(V \cos \theta)} = \frac{M^2 \cos \theta \sin \theta \mp \sqrt{M^2 - 1}}{1 - M^2 \sin^2 \theta}.$$

This simplifies (cancel V and use standard trig identities) to the *differential compatibility equation*

$$\boxed{d\theta = \pm \sqrt{M^2 - 1} \frac{dV}{V}} \iff \begin{cases} C^- : & d\theta = -\sqrt{M^2 - 1} \frac{dV}{V}, \\ C^+ : & d\theta = \sqrt{M^2 - 1} \frac{dV}{V}. \end{cases} \quad (26)$$

Integration introduces the Prandtl–Meyer function

$$\nu(M) = \sqrt{\frac{\gamma + 1}{\gamma - 1}} \tan^{-1} \sqrt{\frac{\gamma - 1}{\gamma + 1} (M^2 - 1)} - \tan^{-1} \sqrt{M^2 - 1}, \quad (27)$$

leading to the *algebraic* compatibility (Riemann invariant) forms

$$\boxed{\theta + \nu(M) = K_- \quad (\text{constant along } C^-)}, \quad \boxed{\theta - \nu(M) = K_+ \quad (\text{constant along } C^+)}. \quad (28)$$

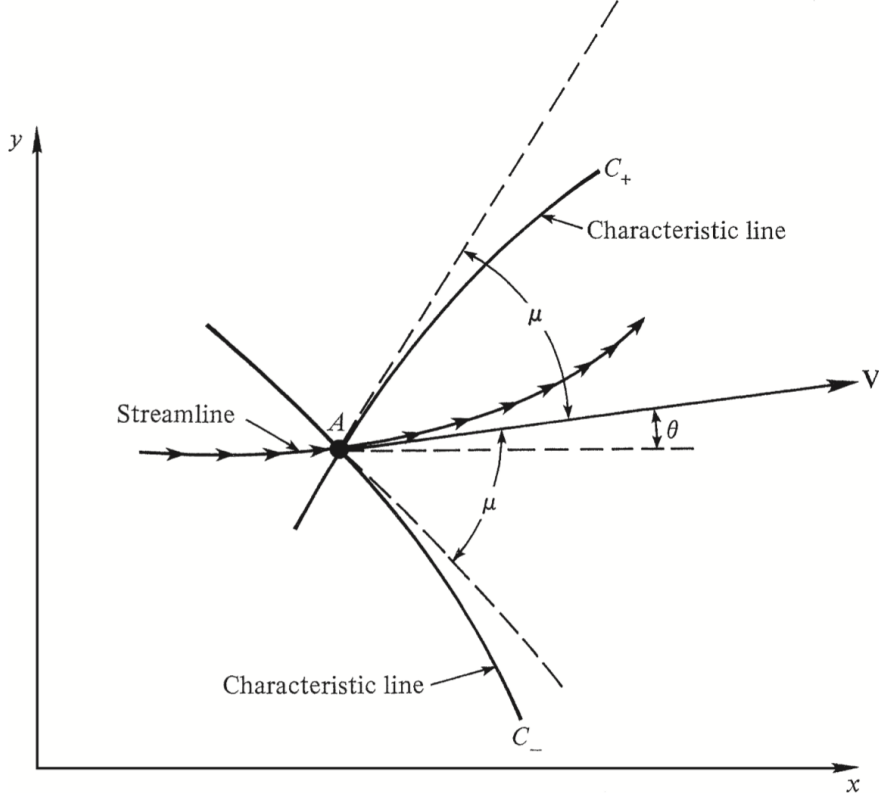


Figure 4: Left- and right-running characteristic lines at a point A : slopes $\tan(\theta \pm \mu)$.

3.4 Unit processes (steady 2D, irrotational)

The compatibility equations and slopes allow marching by a few reusable updates.

(U1) Internal point (C_1^- with C_2^+). Given point 1 with (θ_1, ν_1) and point 2 with (θ_2, ν_2) ,

$$\begin{aligned} \text{from } C^-: \theta_1 + \nu_1 &= K_- = \theta_3 + \nu_3, \\ \text{from } C^+: \theta_2 - \nu_2 &= K_+ = \theta_3 - \nu_3, \end{aligned} \quad (29)$$

so

$$\boxed{\theta_3 = \frac{1}{2}[(\theta_1 + \nu_1) + (\theta_2 - \nu_2)], \quad \nu_3 = \frac{1}{2}[(\theta_1 + \nu_1) - (\theta_2 - \nu_2)].} \quad (30)$$

The location (x_3, y_3) is found by intersecting straight C^- and C^+ segments drawn with *average* angles (Fig. 6):

$$m_{1 \rightarrow 3} = \tan\left(\frac{\theta_1 + \theta_3}{2} - \frac{\nu_1 + \nu_3}{2}\right), \quad m_{2 \rightarrow 3} = \tan\left(\frac{\theta_2 + \theta_3}{2} + \frac{\nu_2 + \nu_3}{2}\right).$$

(U2) Wall point (C_4^- to a solid wall). If interior point 4 sends a C^- to the wall at point 5 whose tangent angle is $\theta_5 = \theta_w$,

$$\boxed{\theta_4 + \nu_4 = K_- = \theta_5 + \nu_5 \implies \nu_5 = \nu_4 + \theta_4 - \theta_w.} \quad (31)$$

(U3) Shock point (if present). Across a shock, K_\pm are *not* conserved. For a point 6 just upstream of a shock, the C^+ invariant is

$$(K_+)_6 = \theta_6 - \nu_6 = (K_+)_7 = \theta_7 - \nu_7, \quad (32)$$

and oblique-shock relations (Chap. 4) determine the post-shock state at point 7 for a trial shock angle β_7 .

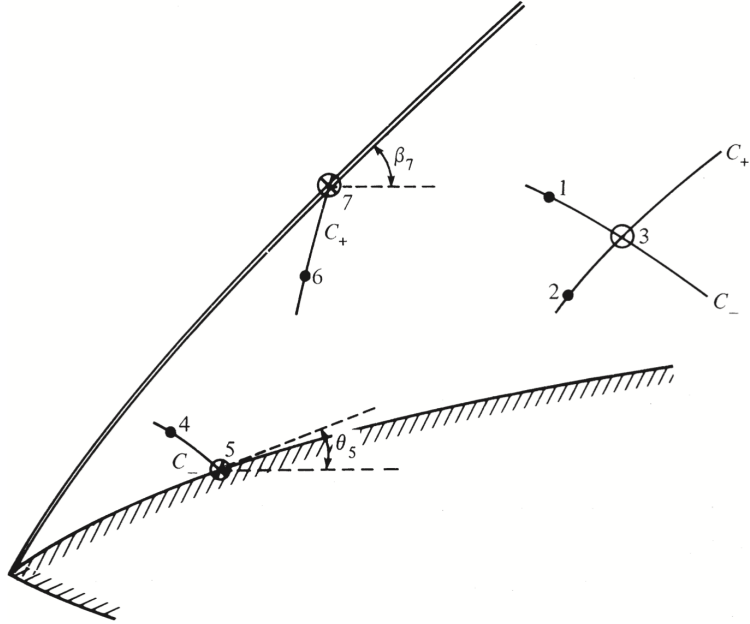


Figure 5: Unit processes: internal intersection (1–2–3), wall point (4–5), and optional shock point (6–7).

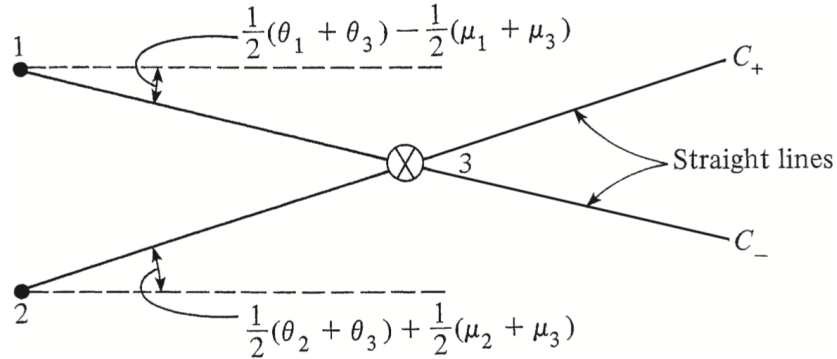


Figure 6: Straight-line approximation for characteristics using average angles.

4 Supersonic nozzle design

We showed that the steady, adiabatic, two-dimensional, irrotational equations are hyperbolic for $M > 1$ and that information travels along the *characteristic lines* with slopes

$$\frac{dy}{dx} \Big|_{C^\pm} = \tan(\theta \pm \mu), \quad \sin \mu = \frac{1}{M}, \quad (33)$$

and that the *compatibility relations* (Riemann invariants) are

$$K^+ \equiv \theta + \nu(M) = \text{const along } C^-, \quad K^- \equiv \theta - \nu(M) = \text{const along } C^+, \quad (34)$$

where the Prandtl–Meyer function is

$$\nu(M) = \sqrt{\frac{\gamma+1}{\gamma-1}} \tan^{-1} \sqrt{\frac{\gamma-1}{\gamma+1}(M^2-1)} - \tan^{-1} \sqrt{M^2-1}. \quad (35)$$

4.1 What has to be designed?

Quasi-one-dimensional relations prescribe how p, ρ, T, M vary with local area ratio A/A^* , but say nothing about the *shape* $A(x)$ of a two-dimensional nozzle. If the contour is not chosen properly, the internal wave pattern (families C^+ and C^-) will not cancel and shocks will develop. The method of characteristics (MOC) gives a constructive way to lay out a contour that yields shock-free, isentropic, uniform, parallel flow at the exit.

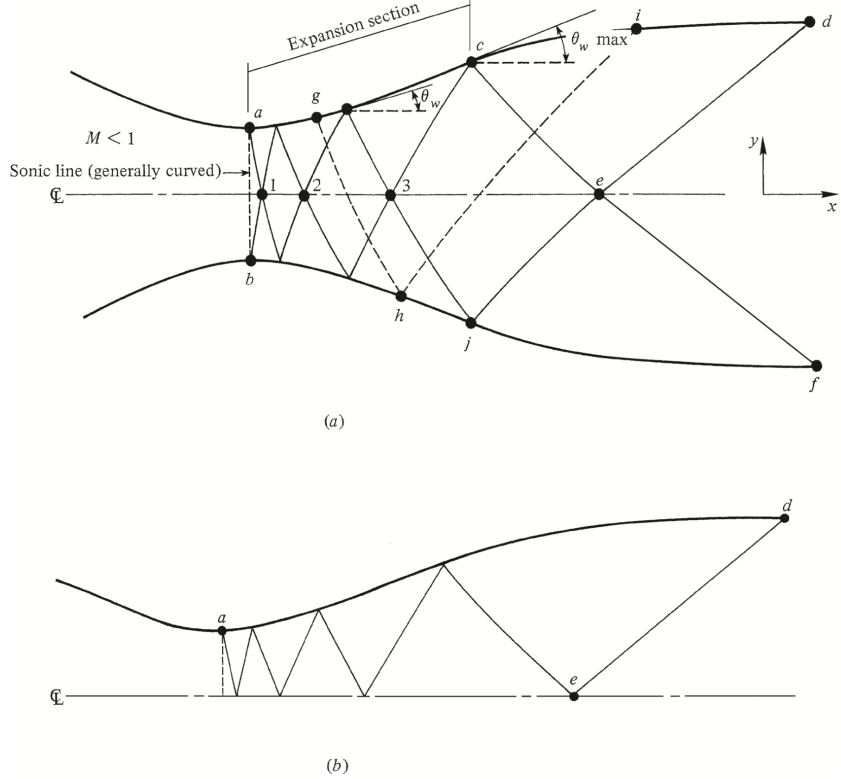


Figure 7: Schematic MOC nozzle layouts. (a) A general nozzle with a finite, gently curved *expansion section* followed by a *straightening section*; (b) by symmetry we can compute only the half-plane above the centerline.

4.2 Minimum-length (ML) nozzle: key result and proof

A particularly important limit is the *minimum-length nozzle* in which the curved expansion is collapsed to a sharp corner at the throat. All the expansion then emanates from a single point (Fig. 8a), and only one right-running and one left-running fan exist. Let the design exit Mach number be M_e and $\nu_M \equiv \nu(M_e)$.

Consider the C^+ line that runs from the wall inflection point c to the centerline point e (Fig. 8b). At e the desired flow is uniform and parallel, hence $\theta_e = 0$ and $\nu_e = \nu_M$. From (34), along this C^+ we have

$$(K^-)_c = \theta_c - \nu_c = \theta_e - \nu_e = -\nu_M. \quad (36)$$

In the ML nozzle we take c at the end of the expansion process and choose $\theta_c = 0$; therefore $\nu_c = \nu_M$ and (36) reads

$$(K^-)_c = -\nu_M. \quad (37)$$

Now follow the C^- line from the throat corner a to c . Invariants give

$$(K^-)_a = (K^-)_c = -\nu_M, \quad \Rightarrow \quad \theta_a - \nu_a = -\nu_M. \quad (38)$$

At the throat just upstream we have sonic, straight flow ($\theta = 0, \nu = 0$). After the sharp turn through the maximum wall angle $\theta_{w,\max,ML}$, the local flow angle and Prandtl–Meyer function at a are equal to that turning: $\theta_a = \nu_a = \theta_{w,\max,ML}$. Substituting in (38) yields the classic ML condition

$$\boxed{\theta_{w,\max,ML} = \frac{\nu_M}{2}} \quad (39)$$

i.e. the maximum wall turn downstream of the throat equals one-half of the Prandtl–Meyer angle for the design exit Mach number.

For air ($\gamma = 1.4$) and, e.g., $M_e = 3.05$ we have

$$\nu_M = \nu(3.05) = 50.712^\circ, \quad \theta_{w,\max,ML} = \nu_M/2 = 25.356^\circ, \quad \mu_e = \sin^{-1} \frac{1}{M_e} = 19.139^\circ.$$

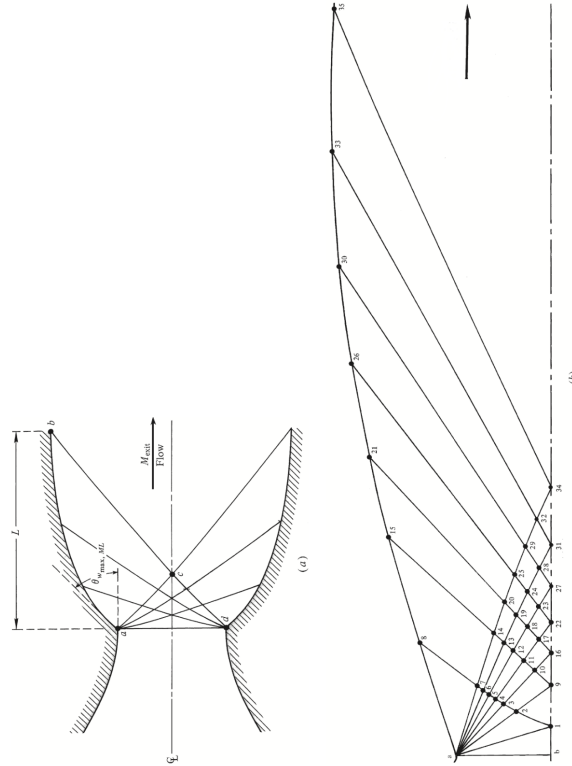


Figure 8: Minimum-length nozzle. (a) Geometry with a single expansion fan from the throat corner; (b) characteristic net used to construct the wall.

4.3 Constructing the ML contour by marching

We discretize the centered expansion fan into N rays with equal increments $\Delta\nu = \nu_M/N$. At the throat corner (start of the fan),

$$\theta_i = \nu_i = i \Delta\nu, \quad (K^+)_i = \theta_i + \nu_i = 2\nu_i, \quad (K^-)_i = \theta_i - \nu_i = 0, \quad i = 1, \dots, N. \quad (40)$$

The remainder of the field is obtained with the unit processes of Sec. 3:

Internal point (intersection of C_1^- and C_2^+). Given points 1 and 2 with known (θ_1, ν_1) and (θ_2, ν_2) ,

$$\theta_3 = \frac{1}{2}[(\theta_1 + \nu_1) + (\theta_2 - \nu_2)], \quad (41)$$

$$\nu_3 = \frac{1}{2}[(\theta_1 + \nu_1) - (\theta_2 - \nu_2)], \quad (42)$$

and M_3 follows from ν_3 via (35). To place (x_3, y_3) we intersect two straight segments drawn with average angles (Fig. 8b):

$$\text{slope } 1 \rightarrow 3 : \tan\left(\frac{\theta_1+\theta_3}{2} - \frac{\mu_1+\mu_3}{2}\right), \quad (43)$$

$$\text{slope } 2 \rightarrow 3 : \tan\left(\frac{\theta_2+\theta_3}{2} + \frac{\mu_2+\mu_3}{2}\right). \quad (44)$$

Wall point (incoming C^- hits the wall). Let point 4 be an interior point whose C^- meets the wall at point 5. Impose the wall tangent $\theta_5 = \theta_w$ and use the invariant along C^- :

$$\nu_5 = (\theta_4 + \nu_4) - \theta_w, \quad M_5 = \nu^{-1}(\nu_5). \quad (45)$$

The location (x_5, y_5) is found by intersecting the straight C^- from 4 (with average angle as above) and the wall line.

Axis reflection. When a characteristic hits the symmetry axis, set $\theta = 0$. The reflected characteristic leaves with the appropriate invariant from (34).

By marching these unit processes—fan rays from the throat corner to the axis, reflections from the axis to the opposite wall, and then the straightening region—the ML wall is obtained. The straightening is complete when the last C^+ from the axis meets the wall with

$$\theta_e = 0, \quad \nu_e = \nu_M, \quad M_e = \nu^{-1}(\nu_M), \quad (46)$$

which guarantees uniform, parallel exit flow at the design Mach number.

4.4 General (non-ML) nozzles

If a finite, gently curved *expansion section* is desired, prescribe an increasing wall angle $\theta_w(x)$ from the throat up to the inflection c . Launch C^- characteristics from this wall, reflect C^+ from the axis, and then design a *straightening section* where θ_w is decreased back to zero so that the remaining waves cancel at the exit. The marching formulas and placement rules are the same as in the ML case, except the starting boundary is a curve rather than a point.

4.5 Practical notes

- Use straight-line characteristics with *average* angles between nodes; this simple second-order treatment is standard and accurate for typical nozzle grids (see Fig. 8b).
- Choose a sufficiently fine fan (N large enough) to avoid a visibly faceted wall. A C^1 spline may be fitted through the wall points, preserving end slopes $\theta_w(0) = \theta_{w,\max}$ and $\theta_w(L) = 0$.
- For wind-tunnel nozzles one often uses a long, gentle expansion (Fig. 7a) to maximize flow quality; for rocket and laser nozzles a short ML layout is preferred to minimize length and weight.

5 Hand Calculation of the First Five MOC Nodes

This section reproduces by hand the first five grid points of the method of characteristics (MOC) solution that our MATLAB code generated for a minimum-length nozzle with $\gamma = 1.4$, design exit Mach number $M_e = 3.05$, and throat radius $R_* = 0.11064$ (same symbols as in the code).

How to obtain the physical throat radius R_*

The characteristic net is built in non-dimensional (x, y) with the throat half-height scaled to unity ($D \equiv y_{\text{wall,th}} = 1$). Converting to physical dimensions requires a single length scale—the *throat radius* R_* . There are three equivalent, practical ways to determine R_* .

Route A: From the (computed) exit area ratio and a chosen exit size. The MOC solution returns the geometric area ratio

$$\frac{A_e}{A_t} = \left(\frac{R_e}{R_*} \right)^2 \implies R_* = \frac{R_e}{\sqrt{A_e/A_t}}.$$

$A_e/A_t = 20.422969$ and the desired exit radius is $R_e = 0.500000$ (units). Hence

$$\sqrt{\frac{A_e}{A_t}} = 4.51978, \quad R_* = \frac{0.500000}{4.51978} = 0.110640 \text{ units.}$$

This is exactly the value used to dimensionize the grid in Sec. 5.

Route B: From the non-dimensional exit height produced by the MOC mesh. Let $y_e^{(\text{nd})}$ be the non-dimensional exit wall radius returned by the march (it equals $\sqrt{A_e/A_t}$ for an axisymmetric nozzle). Because physical $Y = R_* y^{(\text{nd})}$, we have

$$R_* = \frac{R_e}{y_e^{(\text{nd})}}.$$

Our solution gives $y_e^{(\text{nd})} = 4.51978$; with $R_e = 0.500000$,

$$R_* = \frac{0.500000}{4.51978} = 0.110640 \text{ units.}$$

Route C: From required mass flow and chamber conditions (choked flow). When the nozzle is perfectly expanded, the throat is sonic ($M = 1$). The choked mass flux is

$$G^* = \frac{p_0}{\sqrt{T_0}} \sqrt{\frac{\gamma}{R}} \left(\frac{2}{\gamma + 1} \right)^{\frac{\gamma+1}{2(\gamma-1)}},$$

so that

$$A_t = \frac{\dot{m}}{G^*}, \quad R_* = \sqrt{\frac{A_t}{\pi}} = \sqrt{\frac{1}{\pi} \frac{\dot{m}}{p_0} \sqrt{\frac{T_0}{\gamma/R}} \left(\frac{\gamma + 1}{2} \right)^{\frac{\gamma+1}{2(\gamma-1)}}}.$$

Given $(\dot{m}, p_0, T_0, \gamma, R)$ this yields A_t and hence R_* , after which the entire MOC mesh scales as $X = R_* x$ and $Y = R_* y$.

Summary. In practice you will usually: (i) run the MOC once to obtain A_e/A_t , (ii) pick a convenient physical R_e (or overall length scale), and then (iii) use $R_* = R_e/\sqrt{A_e/A_t}$ to dimensionize all coordinates.

Setup

- Exit Prandtl–Meyer angle (from the design M_e):

$$\nu_e = 50.7127^\circ.$$

- Minimum-length expansion fan total turn:

$$\theta_{\max} = \frac{\nu_e}{2} = 25.35635^\circ.$$

- Discretization into $n = 10$ rays (the first row of nodes):

$$\Delta\theta = \frac{\theta_{\max}}{n} = 2.535635^\circ, \quad \theta_i = i \Delta\theta, \quad \nu_i = \theta_i \quad (i = 1, \dots, 10).$$

Hence along this fan,

$$K_i^- = \theta_i - \nu_i = 0, \quad K_i^+ = \theta_i + \nu_i = 2\theta_i.$$

- Mach angle at node i : $\mu_i = \sin^{-1}(1/M_i)$ (in degrees).

- Slopes (all angles in degrees):

$$m_i^- = \tan(\theta_i - \mu_i), \quad m_{i-1,i}^- = \tan\left(\frac{(\theta_{i-1} + \mu_{i-1}) + (\theta_i + \mu_i)}{2}\right).$$

- Geometry for the first row (non-dimensional throat half-height $D = 1$):

$$\text{Node 1: } x_1 = -\frac{D}{m_1^-}, \quad y_1 = 0.$$

$$\text{Node } i \geq 2 : \quad x_i = \frac{D - y_{i-1} + m_{i-1,i}^- x_{i-1}}{m_{i-1,i}^- - m_i^-}, \quad y_i = m_i^- x_i + D.$$

- Dimensional coordinates: $X_i = R_* x_i$, $Y_i = R_* y_i$.

Node-by-node calculations

Node 1

$$\theta_1 = \nu_1 = 2.535635^\circ, \quad M_1 = 1.156855, \quad \mu_1 = \sin^{-1}\left(\frac{1}{M_1}\right) = 59.8157^\circ.$$

Slope and coordinates:

$$m_1^- = \tan(\theta_1 - \mu_1) = \tan(-57.2801^\circ) = -1.54608, \quad x_1 = -\frac{1}{m_1^-} = 0.64666, \quad y_1 = 0.$$

Dimensional:

$$X_1 = 0.11064 \times 0.64666 = 0.07108, \quad Y_1 = 0.$$

Invariants: $K_1^- = 0$, $K_1^+ = 2\theta_1 = 5.07127^\circ$.

Node 2

$$\theta_2 = \nu_2 = 5.071270^\circ, \quad M_2 = 1.25922, \quad \mu_2 = 52.5771^\circ.$$

$$m_2^- = \tan(\theta_2 - \mu_2) = \tan(-47.5058^\circ) = -1.08936, \quad m_{1,2}^- = \tan\left(\frac{(\theta_1 + \mu_1) + (\theta_2 + \mu_2)}{2}\right) = \tan(59.9990^\circ) = 1.73204.$$

Coordinates:

$$x_2 = \frac{1 - y_1 + m_{1,2}^- x_1}{m_{1,2}^- - m_2^-} = \frac{1 + 1.73204 \times 0.64666}{1.73204 - (-1.08936)} = 0.74825,$$

$$y_2 = m_2^- x_2 + 1 = -1.08936 \times 0.74825 + 1 = 0.81698.$$

Dimensional:

$$X_2 = 0.11064 \times 0.74825 = 0.08279, \quad Y_2 = 0.11064 \times 0.81698 = 0.09036.$$

Invariants: $K_2^- = 0$, $K_2^+ = 10.14254^\circ$.

Node 3

$$\theta_3 = \nu_3 = 7.606905^\circ, \quad M_3 = 1.35161, \quad \mu_3 = 47.7181^\circ.$$

$$m_3^- = \tan(7.6069 - 47.7181)^\circ = \tan(-40.1112^\circ) = -0.84480, \quad m_{2,3}^- = \tan\left(\frac{(\theta_2 + \mu_2) + (\theta_3 + \mu_3)}{2}\right) = \tan(56.48^\circ)$$

$$x_3 = \frac{1 - y_2 + m_{2,3}^- x_2}{m_{2,3}^- - m_3^-} = \frac{1 - 0.81698 + 1.50970 \times 0.74825}{1.50970 - (-0.84480)} = 0.82762,$$

$$y_3 = m_3^- x_3 + 1 = -0.84480 \times 0.82762 + 1 = 0.30299.$$

Dimensional:

$$X_3 = 0.11064 \times 0.82762 = 0.09156, \quad Y_3 = 0.11064 \times 0.30299 = 0.03351.$$

Invariants: $K_3^- = 0, K_3^+ = 15.21381^\circ$.

Node 4

$$\theta_4 = \nu_4 = 10.142540^\circ, \quad M_4 = 1.43994, \quad \mu_4 = 43.9880^\circ.$$

$$m_4^- = \tan(10.1425 - 43.9880)^\circ = \tan(-33.8455^\circ) = -0.67133, \quad m_{3,4}^- = \tan\left(\frac{(\theta_3 + \mu_3) + (\theta_4 + \mu_4)}{2}\right) = \tan(54.7^\circ)$$

$$x_4 = \frac{1 - y_3 + m_{3,4}^- x_3}{m_{3,4}^- - m_4^-} = \frac{1 - 0.30299 + 1.40415 \times 0.82762}{1.40415 - (-0.67133)} = 0.89565,$$

$$y_4 = m_4^- x_4 + 1 = -0.67133 \times 0.89565 + 1 = 0.39932.$$

Dimensional:

$$X_4 = 0.11064 \times 0.89565 = 0.09910, \quad Y_4 = 0.11064 \times 0.39932 = 0.04418.$$

Invariants: $K_4^- = 0, K_4^+ = 20.28508^\circ$.

Node 5

$$\theta_5 = \nu_5 = 12.678175^\circ, \quad M_5 = 1.52619, \quad \mu_5 = 40.9362^\circ.$$

$$m_5^- = \tan(12.6782 - 40.9362)^\circ = \tan(-28.2580^\circ) = -0.53676, \quad m_{4,5}^- = \tan\left(\frac{(\theta_4 + \mu_4) + (\theta_5 + \mu_5)}{2}\right) = \tan(53.5^\circ)$$

$$x_5 = \frac{1 - y_4 + m_{4,5}^- x_4}{m_{4,5}^- - m_5^-} = \frac{1 - 0.39932 + 1.34304 \times 0.89565}{1.34304 - (-0.53676)} = 0.95822,$$

$$y_5 = m_5^- x_5 + 1 = -0.53676 \times 0.95822 + 1 = 0.48493.$$

Dimensional:

$$X_5 = 0.11064 \times 0.95822 = 0.10602, \quad Y_5 = 0.11064 \times 0.48493 = 0.05366.$$

Invariants: $K_5^- = 0, K_5^+ = 25.35635^\circ$.

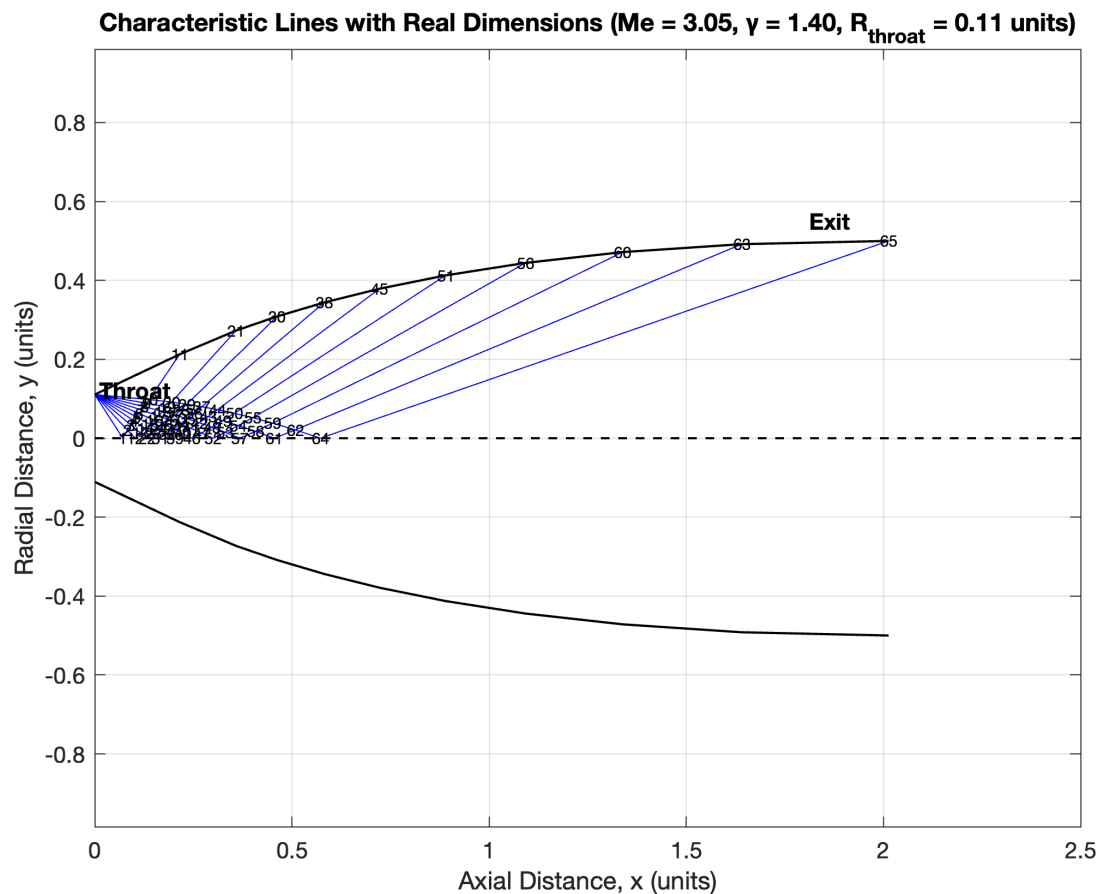
Summary

Node	θ ($^\circ$)	ν ($^\circ$)	M	μ ($^\circ$)	x	y	X	Y	K^-	K^+ ($^\circ$)
1	2.5356	2.5356	1.1569	59.8157	0.64666	0.00000	0.07108	0.00000	0	5.0713
2	5.0713	5.0713	1.2592	52.5771	0.74825	0.81698	0.08279	0.09036	0	10.1425
3	7.6069	7.6069	1.3516	47.7181	0.82762	0.30299	0.09156	0.03351	0	15.2138
4	10.1425	10.1425	1.4399	43.9880	0.89565	0.39932	0.09910	0.04418	0	20.2851
5	12.6782	12.6782	1.5262	40.9362	0.95822	0.48493	0.10602	0.05366	0	25.3563

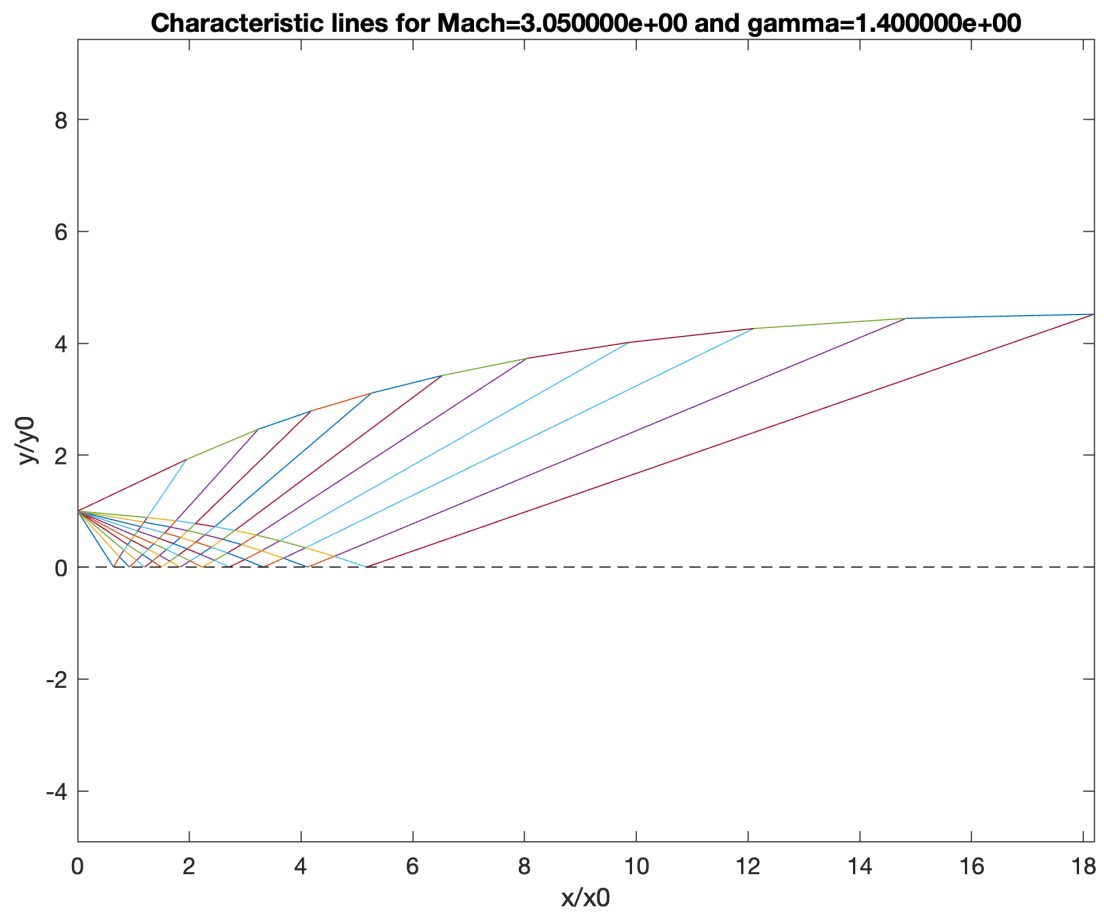
The recipe above (average-slope straight segments with K^\pm invariants) is exactly the one implemented in your script; repeating the same steps yields the next rows (internal intersections, wall points, and axis reflections) in the characteristic net.

NODE PROPERTIES (ALL NODES)								
Node	X	Y	Theta(°)	Mach	μ (°)	v (rad)	KL	KR
1	0.0711	0.0000	2.5356	1.1569	59.8157	2.5356	0.0000	5.0713
2	0.0828	0.0203	5.0713	1.2592	52.5771	5.0713	0.0000	10.1425
3	0.0916	0.0335	7.6069	1.3516	47.7181	7.6069	0.0000	15.2138
4	0.0991	0.0442	10.1425	1.4399	43.9880	10.1425	0.0000	20.2851
5	0.1060	0.0537	12.6782	1.5262	40.9362	12.6782	0.0000	25.3563
6	0.1126	0.0626	15.2138	1.6120	38.3429	15.2138	0.0000	30.4276
7	0.1190	0.0712	17.7494	1.6979	36.0824	17.7494	0.0000	35.4989
8	0.1252	0.0799	20.2851	1.7848	34.0756	20.2851	0.0000	40.5702
9	0.1315	0.0888	22.8207	1.8730	32.2689	22.8207	0.0000	45.6414
10	0.1378	0.0979	25.3563	1.9631	30.6244	25.3563	0.0000	50.7127
11	0.2152	0.2126	25.3563	1.9631	30.6244	25.3563	0.0000	50.7127
12	0.1025	0.0000	0.0000	1.4399	43.9880	10.1425	-10.1425	10.1425
13	0.1164	0.0132	2.5356	1.5262	40.9362	12.6782	-10.1425	15.2138
14	0.1285	0.0247	5.0713	1.6120	38.3429	15.2138	-10.1425	20.2851
15	0.1398	0.0354	7.6069	1.6979	36.0824	17.7494	-10.1425	25.3563
16	0.1507	0.0460	10.1425	1.7848	34.0756	20.2851	-10.1425	30.4276
17	0.1615	0.0566	12.6782	1.8730	32.2689	22.8207	-10.1425	35.4989
18	0.1724	0.0676	15.2138	1.9631	30.6244	25.3563	-10.1425	40.5702
19	0.1834	0.0792	17.7494	2.0553	29.1141	27.8920	-10.1425	45.6414
20	0.1948	0.0916	20.2851	2.1501	27.7165	30.4276	-10.1425	50.7127
21	0.3578	0.2726	20.2851	2.1501	27.7165	30.4276	-10.1425	50.7127
22	0.1331	0.0000	0.0000	1.6120	38.3429	15.2138	-15.2138	15.2138
23	0.1480	0.0118	2.5356	1.6979	36.0824	17.7494	-15.2138	20.2851
24	0.1621	0.0232	5.0713	1.7848	34.0756	20.2851	-15.2138	25.3563
25	0.1759	0.0346	7.6069	1.8730	32.2689	22.8207	-15.2138	30.4276
26	0.1897	0.0463	10.1425	1.9631	30.6244	25.3563	-15.2138	35.4989
27	0.2038	0.0587	12.6782	2.0553	29.1141	27.8920	-15.2138	40.5702
28	0.2182	0.0719	15.2138	2.1501	27.7165	30.4276	-15.2138	45.6414
29	0.2333	0.0862	17.7494	2.2478	26.4151	32.9633	-15.2138	50.7127
30	0.4624	0.3087	17.7494	2.2478	26.4151	32.9633	-15.2138	50.7127
31	0.1656	0.0000	0.0000	1.7848	34.0756	20.2851	-20.2851	20.2851
32	0.1826	0.0116	2.5356	1.8730	32.2689	22.8207	-20.2851	25.3563
33	0.1995	0.0235	5.0713	1.9631	30.6244	25.3563	-20.2851	30.4276
34	0.2165	0.0360	7.6069	2.0553	29.1141	27.8920	-20.2851	35.4989
35	0.2341	0.0494	10.1425	2.1501	27.7165	30.4276	-20.2851	40.5702
36	0.2523	0.0639	12.6782	2.2478	26.4151	32.9633	-20.2851	45.6414
37	0.2715	0.0799	15.2138	2.3489	25.1967	35.4989	-20.2851	50.7127
38	0.5817	0.3440	15.2138	2.3489	25.1967	35.4989	-20.2851	50.7127
39	0.2026	0.0000	0.0000	1.9631	30.6244	25.3563	-25.3563	25.3563
40	0.2227	0.0121	2.5356	2.0553	29.1141	27.8920	-25.3563	30.4276
41	0.2434	0.0251	5.0713	2.1501	27.7165	30.4276	-25.3563	35.4989
42	0.2648	0.0393	7.6069	2.2478	26.4151	32.9633	-25.3563	40.5702
43	0.2874	0.0549	10.1425	2.3489	25.1967	35.4989	-25.3563	45.6414
44	0.3114	0.0724	12.6782	2.4537	24.0505	38.0345	-25.3563	50.7127
45	0.7221	0.3788	12.6782	2.4537	24.0505	38.0345	-25.3563	50.7127
46	0.2464	0.0000	0.0000	2.1501	27.7165	30.4276	-30.4276	30.4276
47	0.2710	0.0133	2.5356	2.2478	26.4151	32.9633	-30.4276	35.4989
48	0.2969	0.0280	5.0713	2.3489	25.1967	35.4989	-30.4276	40.5702
49	0.3244	0.0445	7.6069	2.4537	24.0505	38.0345	-30.4276	45.6414
50	0.3540	0.0632	10.1425	2.5627	22.9677	40.5702	-30.4276	50.7127
51	0.8899	0.4127	10.1425	2.5627	22.9677	40.5702	-30.4276	50.7127
52	0.3000	0.0000	0.0000	2.3489	25.1967	35.4989	-35.4989	35.4989
53	0.3310	0.0150	2.5356	2.4537	24.0505	38.0345	-35.4989	40.5702
54	0.3642	0.0322	5.0713	2.5627	22.9677	40.5702	-35.4989	45.6414
55	0.4003	0.0520	7.6069	2.6763	21.9410	43.1058	-35.4989	50.7127
56	1.0924	0.4443	7.6069	2.6763	21.9410	43.1058	-35.4989	50.7127
57	0.3676	0.0000	0.0000	2.5627	22.9677	40.5702	-40.5702	40.5702
58	0.4076	0.0175	2.5356	2.6763	21.9410	43.1058	-40.5702	45.6414
59	0.4514	0.0382	5.0713	2.7950	20.9641	45.6414	-40.5702	50.7127
60	1.3388	0.4717	5.0713	2.7950	20.9641	45.6414	-40.5702	50.7127
61	0.4553	0.0000	0.0000	2.7950	20.9641	45.6414	-45.6414	45.6414
62	0.5083	0.0212	2.5356	2.9194	20.0318	48.1771	-45.6414	50.7127
63	1.6407	0.4918	2.5356	2.9194	20.0318	48.1771	-45.6414	50.7127
64	0.5722	0.0000	0.0000	3.0500	19.1395	50.7127	-50.7127	50.7127
65	2.0130	0.5000	0.0000	3.0500	19.1395	50.7127	-50.7127	50.7127

Figure 9: Complete *Node Properties (All Nodes)* table produced by the solver.



(a) Characteristic lines with real dimensions.



(b) Non-dimensional characteristic net.

6 Design of the Subsonic Converging Section (Cosine–Bell)

For a short, smooth, separation-free converging passage we adopt the *cosine–bell* (raised–cosine) profile. Let the axial coordinate in the converging section be $x \in [-L_c, 0]$, with $x = -L_c$ at the inlet and $x = 0$ at the throat. Denote inlet and throat radii by R_i and R_t , respectively, and define the non-dimensional arclength parameter

$$s \equiv \frac{x + L_c}{L_c} \in [0, 1], \quad \text{so that } s = 0 \text{ at the inlet and } s = 1 \text{ at the throat.} \quad (47)$$

The cosine–bell radius distribution is then

$$r(s) = R_t + (R_i - R_t) \frac{1 + \cos(\pi s)}{2}, \quad 0 \leq s \leq 1, \quad (48)$$

which satisfies $r(0) = R_i$, $r(1) = R_t$, and has *zero slope* at both ends:

$$\frac{dr}{ds} = -\frac{\pi}{2}(R_i - R_t) \sin(\pi s), \quad \left. \frac{dr}{ds} \right|_{s=0,1} = 0. \quad (49)$$

The wall slope with respect to x is

$$\frac{dr}{dx} = \frac{dr}{ds} \frac{ds}{dx} = -\frac{\pi}{2L_c}(R_i - R_t) \sin(\pi s). \quad (50)$$

Its maximum magnitude occurs at $s = \frac{1}{2}$:

$$\left. \frac{dr}{dx} \right|_{\max} = \frac{\pi}{2L_c}(R_i - R_t). \quad (51)$$

The local wall angle is $\alpha(x) = \arctan(dr/dx)$; hence the **length of the converging section** required to respect a prescribed peak wall angle α_{\max} is

$$L_c = \frac{\pi(R_i - R_t)}{2 \tan \alpha_{\max}}. \quad (52)$$

Conversely, if L_c is chosen first, the resulting peak wall angle is

$$\alpha_{\max} = \arctan\left(\frac{\pi(R_i - R_t)}{2L_c}\right). \quad (53)$$

Optional curvature constraint. The second derivative with respect to x is

$$\frac{d^2r}{dx^2} = -\frac{\pi^2}{2L_c^2}(R_i - R_t) \cos(\pi s), \quad (54)$$

whose magnitude is largest at the ends ($s = 0, 1$). If a curvature limit κ_{\lim} is required near the inlet/throat, a conservative bound is obtained from $|d^2r/dx^2|_{\max} \leq \kappa_{\lim}$, i.e.

$$L_c \geq \frac{\pi}{\sqrt{2}} \sqrt{\frac{R_i - R_t}{\kappa_{\lim}}}. \quad (55)$$

In practice, (52) (slope limit) is the primary sizing relation; (55) can be checked afterward for additional smoothness.

Area and velocity variation. The cross-sectional area and its evolution are

$$A(s) = \pi r(s)^2, \quad \frac{dA}{dx} = 2\pi r \frac{dr}{dx}. \quad (56)$$

For subsonic flow in the converging passage,

$$\dot{m} = \rho V A = \text{const.}$$

When $M \lesssim 0.3$ the density variation is small and $V(x) \approx \dot{m}/(\rho_0 A(x)) \propto 1/A(x)$. If desired, a compressible isentropic update may be used by coupling the subsonic branch of the area–Mach relation to $A(s)$.

Discretization for CAD/CFD. Given a chosen L_c , the profile for tabulation follows from (48) with

$$x_k = -L_c + s_k L_c, \quad s_k = \frac{k}{N} \quad (k = 0, \dots, N), \quad r_k = r(s_k).$$

Worked example (consistent with current nozzle scale). Let the inlet radius be $R_i = 1.0000$ (units), the throat radius $R_t = 0.11064$ (units), and select a smoothness limit $\alpha_{\max} = 25^\circ$ for the peak wall angle in the contraction. Then, from (52),

$$\Delta R = R_i - R_t = 0.88936, \quad L_c = \frac{\pi \Delta R}{2 \tan 25^\circ} \approx \frac{1.5708 \times 0.88936}{0.4663} \approx 3.00 \text{ units.}$$

With this L_c , the maximum slope occurs mid–contraction and the resulting profile is

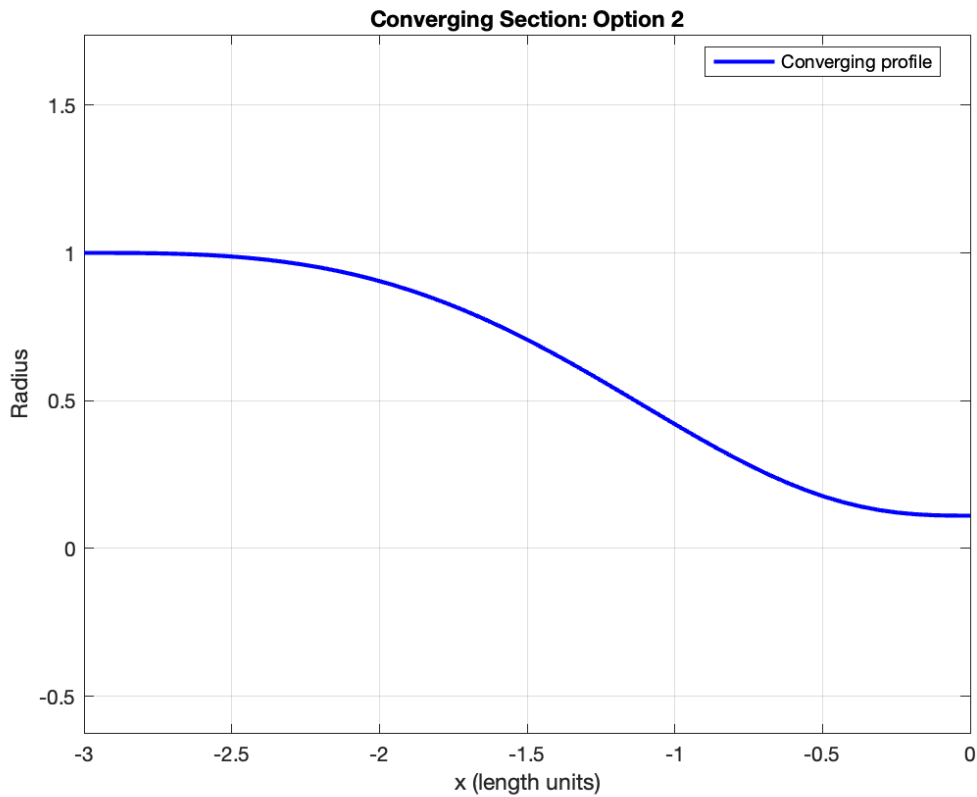
$$r(x) = R_t + (R_i - R_t) \frac{1 + \cos[\pi(x + L_c)/L_c]}{2}, \quad x \in [-3.00, 0].$$

If instead you must fit a prescribed contraction length $L_c = 2.50$ units, the implied peak wall angle is, from (53),

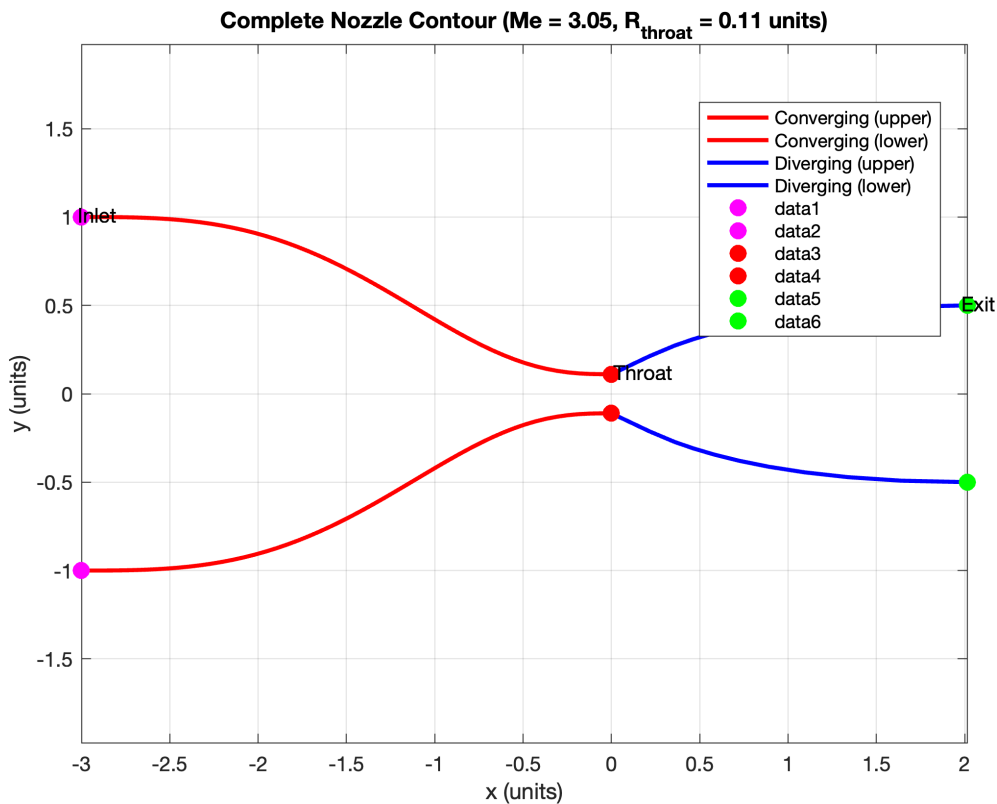
$$\alpha_{\max} = \arctan\left(\frac{\pi(0.88936)}{2 \times 2.50}\right) \approx \arctan(0.558) \approx 29.2^\circ.$$

Choose L_c so that α_{\max} stays within your manufacturing/aerodynamic limits (typical smooth contractions use $15^\circ \lesssim \alpha_{\max} \lesssim 30^\circ$ depending on application).

Joining to the throat. The cosine–bell gives $dr/dx = 0$ at $x = 0^-$, i.e. a *smooth* approach to the throat. If a minimum–length (ML) nozzle is required, the ML supersonic section begins with a *sharp corner* at the throat to launch a centered expansion fan. In that case, either set the converging section length to zero (sharp corner), or blend the smooth contraction into a short circular arc that terminates with the desired corner angle at $x = 0$.



(a) Converging section (Cosine-Bell contraction).



(b) Complete nozzle contour with converging and diverging sections.

Figure 11: Converging profile and resulting complete nozzle contour shown one under the other.

7 CFD Setup and Numerical Method (SU2)

This section documents the computational setup used to verify the minimum-length nozzle designed in §3. All simulations were performed with SU2. Unless otherwise noted, SI units are used and all variables are dimensional.

7.1 Governing equations and turbulence model

We solve the compressible Reynolds-averaged Navier-Stokes (RANS) equations with the Menter SST model (1994 revision) for closure. The choice `SOLVER = RANS` and `KIND_TURB_MODEL = SST` (`V1994m`) provides robust shock/expansion handling and accurate boundary-layer response in nozzles.

7.2 Dimensionalization and initialization

We work in the dimensional framework, `REF_DIMENSIONALIZATION = DIMENSIONAL`, and initialize from thermodynamic (stagnation) conditions:

$$p_0 = \text{FREESTREAM_PRESSURE}, \quad T_0 = \text{FREESTREAM_TEMPERATURE}.$$

A tiny free-stream Mach number (`MACH_NUMBER = 1e-9`) creates a quiescent starting field; the flow is driven by the inlet/outlet boundaries thereafter.

7.3 Fluid model: ideal air vs. non-ideal MDM

For air validations we use `FLUID_MODEL = STANDARD_AIR` (hardcoded $\gamma = 1.4$, $R = 287.058 \times 10^0 \text{ J kg}^{-1} \text{ K}^{-1}$). For the siloxane MDM (octamethyltrisiloxane), we switch to the Peng-Robinson EOS:

$$\begin{aligned} \text{FLUID_MODEL} &= \text{PR_GAS}, \quad p = \frac{RT}{v - b} - \frac{a(T)}{v(v + b) + b(v - b)}, \\ a(T) &= 0.45724 \frac{R^2 T_c^2}{P_c} \alpha(T), \quad b = 0.07780 \frac{RT_c}{P_c}, \quad \alpha(T) = [1 + \kappa(1 - \sqrt{T/T_c})]^2, \\ \kappa &= 0.37464 + 1.54226 \omega - 0.26992 \omega^2, \end{aligned}$$

where (T_c, P_c, ω) are the fluid's critical temperature, critical pressure, and acentric factor, respectively. Temperature-dependent transport may be modelled with polynomial fits:

- `VISCOSITY_MODEL = POLYNOMIAL_VISCOSITY` with coefficients $\mu(T) = \sum_i a_i T^i$,
- `CONDUCTIVITY_MODEL = POLYNOMIAL_CONDUCTIVITY` with $k(T) = \sum_i b_i T^i$.

7.4 Domain, boundaries and operating point

The 2D meridional section is computed with a centerline symmetry condition. The wall is adiabatic and no-slip. At the inlet, we impose total (stagnation) conditions (p_0, T_0) and axial flow direction. At the outlet, we prescribe the back pressure p_b .

For an *ideal-gas* design targeting exit Mach number M_e , a good initial estimate for the shock-free back pressure is the isentropic relation

$$\frac{p_e}{p_0} = \left(1 + \frac{\gamma - 1}{2} M_e^2\right)^{-\gamma/(\gamma-1)}. \quad (57)$$

For $M_e = 3.05$ and $\gamma = 1.4$, (57) gives $p_e/p_0 \approx 2.526 \times 10^{-2}$. With $p_0 = 1.0 \times 10^6 \text{ Pa}$ we start from $p_b \approx 2.5 \times 10^4 \text{ Pa}$ and then adjust slightly: increase p_b if a normal shock forms inside; decrease p_b if the jet is strongly overexpanded at the exit. For MDM (non-ideal), we use the same strategy, but minor tuning of p_b is more frequently required.

Axisymmetric option. For an axisymmetric nozzle computed in a 2D (x, y) slice, activate: `AXISYMMETRIC = YES` with the axis specified by `AXIS_ORIGIN` and `AXIS_DIRECTION`.

7.5 Discretization and numerics

A robust second-order finite-volume scheme is employed:

- Roe flux with entropy fix (`CONV_NUM_METHOD_FLOW = ROE, ENTROPY_FIX_COEFF = 0.1`),
- MUSCL reconstruction (`MUSCL_FLOW = YES`) with a limiter (we recommend `VENKATAKRISHNAN`),
- Implicit Euler time marching for flow and turbulence,
- Krylov linear solver (`FGMRES`) with ILU preconditioner.

The CFL number is ramped adaptively, e.g. from 0.05 to $\mathcal{O}(10)$, to avoid start-up divergence.

7.6 Convergence and outputs

We iterate until the density residual drops by at least 10^{-6} – 10^{-8} (or a maximum of 10^4 iterations). We write volume and surface fields every 100 iterations and monitor residuals plus wall pressure distributions, centerline Mach, and mass flow to verify a parallel, shock-free exit flow.

7.7 Ready-to-run SU2 snippet (edit markers and MDM properties)

```

SOLVER                  = RANS
KIND_TURB_MODEL          = SST
SST_OPTIONS               = V1994m
SYSTEM_MEASUREMENTS      = SI
REF_DIMENSIONALIZATION    = DIMENSIONAL
INIT_OPTION                = TD_CONDITIONS
FREESTREAM_PRESSURE        = 1.0e6
FREESTREAM_TEMPERATURE      = 288.15
MACH_NUMBER                 = 1e-9

% --- Fluid: switch AIR -> PR_GAS for MDM ---
FLUID_MODEL                = PR_GAS
CRITICAL_TEMPERATURE        = <Tc>
CRITICAL_PRESSURE           = <Pc>
ACENTRIC_FACTOR              = <omega>
VISCOSITY_MODEL             = POLYNOMIAL_VISCOSITY
MU_POLY_COEFF                = ( <a0>, <a1>, <a2>, <a3> )
CONDUCTIVITY_MODEL           = POLYNOMIAL_CONDUCTIVITY
K_POLY_COEFF                  = ( <b0>, <b1>, <b2>, <b3> )

% --- Axisymmetric 2-D slice ---
AXISYMMETRIC                = YES
AXIS_ORIGIN                  = ( 0.0, 0.0, 0.0 )
AXIS_DIRECTION                = ( 1.0, 0.0, 0.0 )

% --- Boundaries ---
MARKER_SYM                   = ( SYMMETRY )
MARKER_HEATFLUX                = ( WALL, 0.0 ) %
                                         adiabatic wall
MARKER RIEMANN                  = ( INLET,
                                         TOTAL_CONDITIONS_PT, 1.0e6, 288.15, 1.0, 0.0, 0.0 )
MARKER_OUTLET                  = ( OUTLET, 2.50e4 ) %
                                         start from ideal estimate

```

```

% --- Numerics ---
CONV_NUM_METHOD_FLOW      = ROE
ENTROPY_FIX_COEFF         = 0.1
MUSCL_FLOW                = YES
SLOPE_LIMITER_FLOW        = VENKATAKRISHNAN
TIME_DISCRE_FLOW          = EULER_IMPLICIT
CONV_NUM_METHOD_TURB       = SCALAR_UPWIND
TIME_DISCRE_TURB           = EULER_IMPLICIT
LINEAR_SOLVER              = FGMRES
LINEAR_SOLVER_PREC         = ILU
CFL_NUMBER                 = 0.1
CFL_ADAPT                  = YES
CFL_ADAPT_PARAM            = ( 0.5, 2.0, 0.05, 50.0 )

% --- Convergence & IO ---
ITER                      = 10000
CONV_RESIDUAL_MINVAL       = -6
MESH_FILENAME               = nozzle_xy_conformal.su2
VOLUME_FILENAME             = flow
SURFACE_FILENAME            = surface_flow
OUTPUT_WRT_FREQ              = 100

```

7.8 Verification against the MOC design

The CFD case is consistent with the MOC target M_e by: (i) ensuring the geometric contour exactly matches the derived wall nodes, (ii) setting p_b via (57) and adjusting slightly to remove weak shocks, and (iii) checking that the exit flow is parallel ($\theta_e \approx 0$), with centerline Mach equal to the design value. If the outlet plane shows overexpansion (fan visible at the lip), lower p_b ; if a normal shock sits inside the nozzle, raise p_b .

What to report. For reproducibility, provide: mesh statistics (min/max spacing, first cell height), the exact boundary tags, the final p_b , residual histories, and distributions of M , p and θ along the wall and centerline.

8 CFD Analysis of the Supersonic Nozzle

This section documents the Reynolds-Averaged Navier-Stokes (RANS) simulation of the designed converging-diverging nozzle using SU2. The exact configuration file was summarized earlier; here we explain the modeling choices, write the mathematical formulation solved by the code, and present the main results (contours, centerline trends, and mesh).

8.1 Governing Equations and Models

The solver is RANS with Menter's SST turbulence model:

$$\text{Continuity:} \quad \frac{\partial \rho}{\partial t} + \nabla \cdot (\rho \mathbf{u}) = 0, \quad (58)$$

$$\text{Momentum:} \quad \frac{\partial(\rho \mathbf{u})}{\partial t} + \nabla \cdot (\rho \mathbf{u} \otimes \mathbf{u} + p \mathbf{I}) = \nabla \cdot \boldsymbol{\tau}^{\text{eff}}, \quad (59)$$

$$\text{Total energy:} \quad \frac{\partial(\rho E)}{\partial t} + \nabla \cdot [\mathbf{u} (\rho E + p)] = \nabla \cdot (\boldsymbol{\tau}^{\text{eff}} \cdot \mathbf{u} - \mathbf{q}^{\text{eff}}). \quad (60)$$

The perfect-gas state relation with constant γ is

$$p = (\gamma - 1) \left(\rho E - \frac{1}{2} \rho \|\mathbf{u}\|^2 \right), \quad a = \sqrt{\gamma p / \rho}. \quad (61)$$

The effective viscous stress and heat flux use Boussinesq closure:

$$\boldsymbol{\tau}^{\text{eff}} = (\mu + \mu_t) \left[\nabla \mathbf{u} + (\nabla \mathbf{u})^\top \right] - \frac{2}{3} (\mu + \mu_t) (\nabla \cdot \mathbf{u}) \mathbf{I}, \quad (62)$$

$$\mathbf{q}^{\text{eff}} = -(\lambda + \lambda_t) \nabla T, \quad \lambda_t = \mu_t c_p / \Pr_t, \quad (63)$$

with constant laminar viscosity μ and a constant-Prandtl thermal model as in the configuration.

SST $k-\omega$ model (V1994m). The transport equations solved for the turbulent kinetic energy k and specific dissipation ω read

$$\frac{\partial(\rho k)}{\partial t} + \nabla \cdot (\rho k \mathbf{u}) = P_k - \beta^* \rho k \omega + \nabla \cdot [(\mu + \sigma_k \mu_t) \nabla k], \quad (64)$$

$$\frac{\partial(\rho \omega)}{\partial t} + \nabla \cdot (\rho \omega \mathbf{u}) = \alpha \frac{\omega}{k} P_k - \beta \rho \omega^2 + \nabla \cdot [(\mu + \sigma_\omega \mu_t) \nabla \omega] + 2(1 - F_1) \rho \sigma_{\omega 2} \frac{1}{\omega} \nabla k \cdot \nabla \omega, \quad (65)$$

with eddy viscosity

$$\mu_t = \rho \frac{a_1 k}{\max(a_1 \omega, SF_2)}, \quad (66)$$

where S is a scalar measure of the strain rate and F_1, F_2 are blending functions. Constants are blended between $k-\omega$ and $k-\varepsilon$ limits; SU2 uses the standard Menter values for the selected option V1994m.

In summary, Eqs. (58)–(60) plus (64)–(65), the gas law, and constitutive relations define the PDE system advanced by the code.

8.2 Thermophysical Model and Free-Stream

The configuration employs STANDARD_AIR with $\gamma = 1.4$ and $R = 287.058 \text{ J kg}^{-1} \text{ K}^{-1}$. Initialization is done from thermodynamic (TD_CONDITIONS) variables with free-stream $p_\infty = 1.0 \times 10^6 \text{ Pa}$, $T_\infty = 288.15 \times 10^0 \text{ K}$ and a negligible MACH_NUMBER for the far field (the physical inflow is enforced through the inlet boundary condition described next).

Laminar viscosity is set constant, MU_CONSTANT = $1.716 \times 10^{-5} \text{ kg m}^{-1} \text{ s}^{-1}$. Thermal transport is modeled using a constant-Prandtl closure (the laminar Pr is the code default).

8.3 Boundary Conditions

Three boundary types are used:

- **Inlet (Riemann, total conditions):** MARKER_RIEMANN = (INLET, TOTAL_CONDITIONS_PT, p_0 , T_0 , n_x , n_y , n_z) with $p_0 = 1.0 \times 10^6$ Pa and $T_0 = 288.15 \times 10^0$ K. SU2 converts the total conditions to static using the isentropic relations in the inflow direction:

$$T = \frac{T_0}{1 + \frac{\gamma-1}{2} M^2}, \quad p = p_0 \left(\frac{T}{T_0} \right)^{\frac{\gamma}{\gamma-1}}, \quad \mathbf{u} = Ma \hat{\mathbf{n}}.$$

The inflow Mach follows the characteristic formulation so that the nozzle establishes the correct sonic throat and supersonic core.

- **Outlet (static pressure):** MARKER_OUTLET = (OUTLET, p_{out}) with $p_{out} = 25000 \times 10^0$ Pa, imposing the back pressure that sets the exit expansion level.
- **Walls and symmetry:** MARKER_HEATFLUX = (WALL, 0.0) enforces adiabatic no-slip walls; the centerline uses MARKER_SYM for symmetry.

8.4 Spatial/Temporal Discretization and Solvers

Gradients use Green–Gauss reconstruction (NUM_METHOD_GRAD=GREEN_GAUSS). Convective fluxes are Roe’s approximate Riemann solver with a small entropy fix ($\epsilon = 0.1$). Flow variables are MUSCL–TVD reconstructed (MUSCL_FLOW=YES), second-order in space; limiter is set to NONE for low numerical dissipation in this smooth expansion. Implicit Euler time marching (EULER_IMPLICIT) is employed with an adaptive CFL strategy. The linear system at each step is solved by FGMRES(ILU) with tight residual control.

8.5 Mesh

A body-fitted structured grid (`nozzle_mesh.su2`) is used, refined near the throat and the initial diverging section to resolve strong gradients. The grid is shown in Fig. 12.

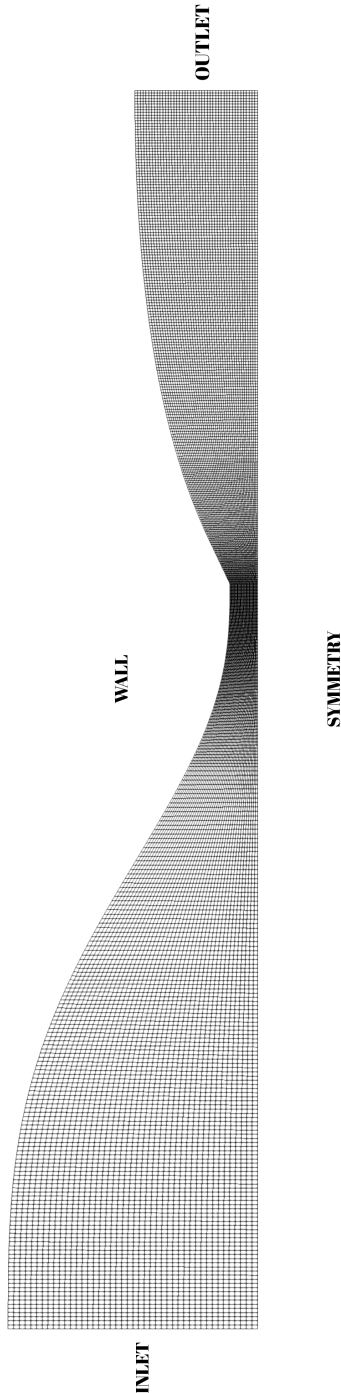
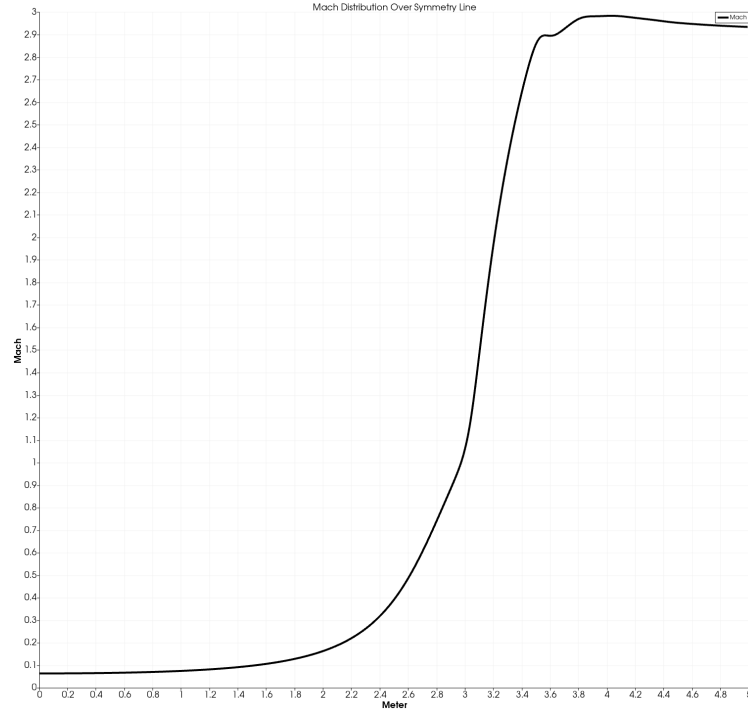


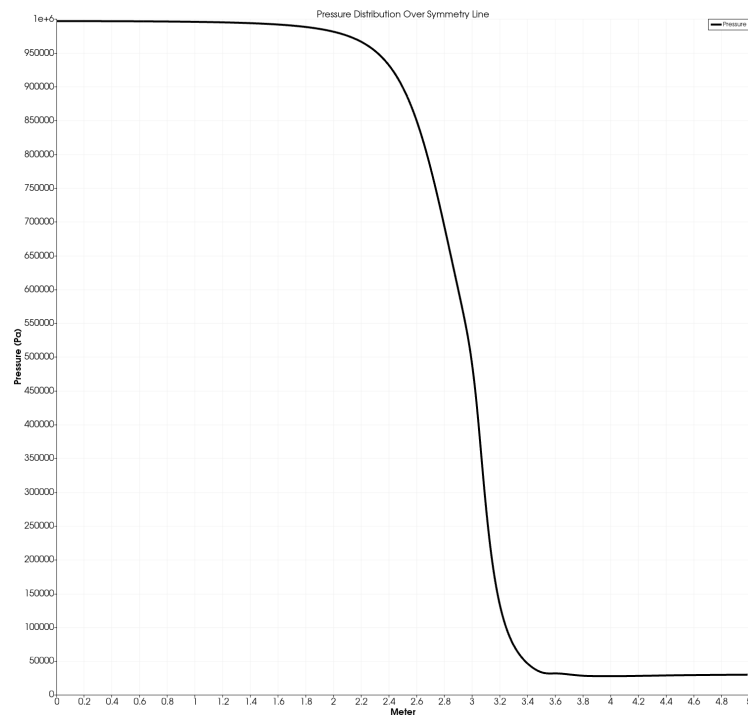
Figure 12: Computational mesh (inlet → throat → exit from bottom to top). Cells are clustered at the throat and early expansion.

8.6 Results

Centerline trends. The symmetry-line (centerline) distributions in Fig. 13 quantify the quasi-one-dimensional behavior: Mach rises steeply through the throat, plateaus in the diverging section near the design value, and the pressure drops from the total inlet level to the outlet back pressure.



(a) Mach number along the symmetry line.



(b) Static pressure (Pa) along the symmetry line.

Figure 13: Centerline evolution from inlet to exit.

Field contours. Figure 14 shows Mach number and static pressure fields. The flow accelerates to $M \approx 1$ at the throat and expands smoothly to a nearly uniform supersonic core toward the exit; pressure falls accordingly and then relaxes toward the back pressure.

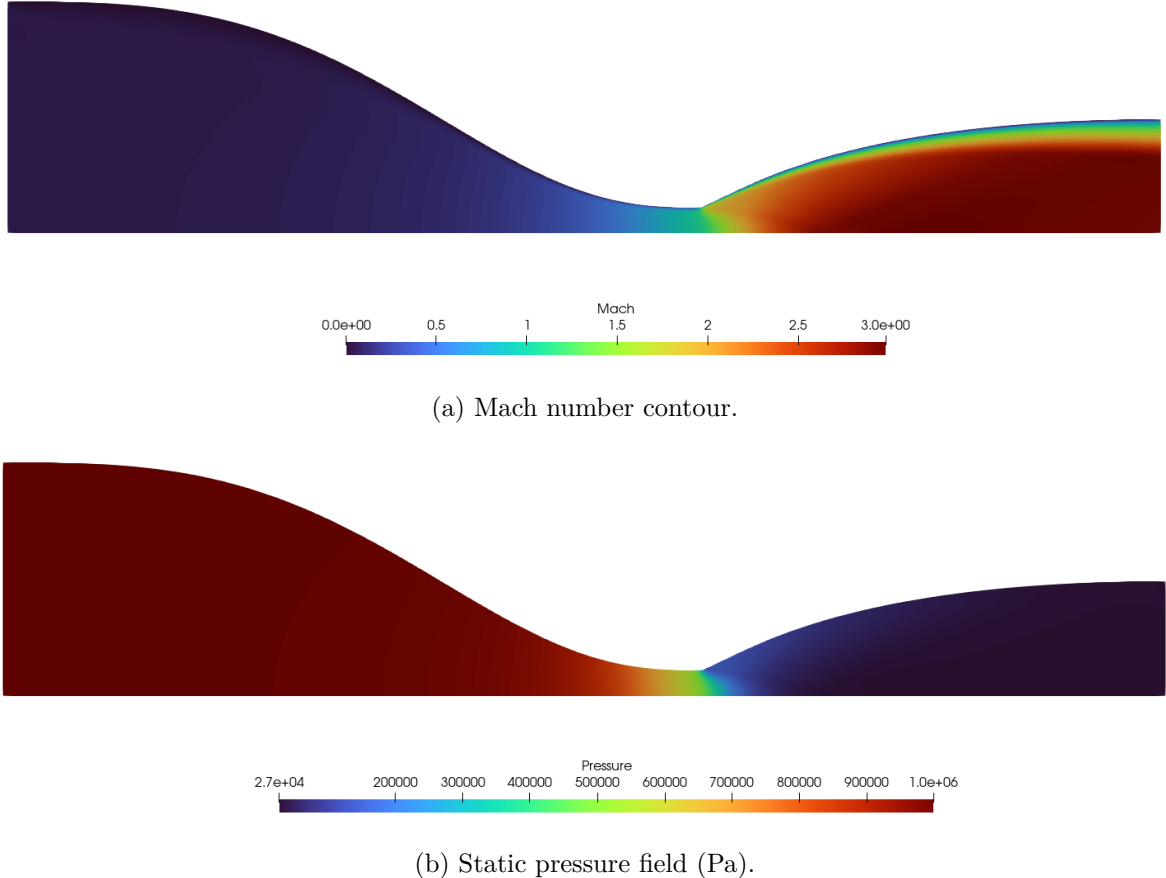


Figure 14: RANS–SST solution: flowfield contours.

Numerical behavior. With the chosen Roe + MUSCL discretization, implicit time stepping, and adaptive CFL, the solver marches to a steady state consistent with the MOC geometry: a shock-free expansion and nearly parallel exit flow.

9 Results and Discussion

9.1 Method of Characteristics (MOC) results

The minimum-length nozzle was synthesized with air ($\gamma = 1.4$) for a target exit Mach number $M_e = 3.05$. The centered fan from the throat was discretized with $N = 10$ rays, giving an initial increment $\Delta\theta = \nu_e/N = 25.35635^\circ/10 = 2.535635^\circ$. Marching with the algebraic invariants $K^+ = \theta + \nu$ (constant on C^-) and $K^- = \theta - \nu$ (constant on C^+) produced a straight-segment characteristic net, wall points, and nodal flow states. The most relevant integral outputs are summarized in Table 1 (numbers correspond to the report generated by the code used in this work).

The complete list of *Node Properties (All Nodes)* (angles, M , K^\pm) was reported earlier and was used to generate the characteristic net and wall locus.

Table 1: Key MOC outputs (design point).

Quantity	Value	Notes
Exit Mach number, M_e	3.0500	by construction
Throat radius, R_t	0.11064 units	from geometry scaling
Diverging length, L_{div}	2.012956 units	min-length solution
Area ratio, A_e/A_t	20.423	from r_e^2/r_t^2
Exit pressure ratio, p_e/p_0	0.025261	isentropic from M_e
Exit temperature ratio, T_e/T_0	0.349589	isentropic from M_e
Max wall turn, $\theta_{w,\max}$	$25.35635^\circ/2 = 12.678175^\circ$	ML condition

9.2 CFD results (SU2, RANS–SST)

A compressible RANS simulation with the SST turbulence model was performed in SU2 using the configuration described in Sec. 8. The domain is the half-nozzle (symmetry about the centerline). Inflow total conditions were $p_0 = 1.0 \times 10^6$ Pa and $T_0 = 288.15$ K; the outlet static pressure was set to 25 kPa to match the isentropic design. The Roe flux with implicit time marching and adaptive CFL was used. The structured mesh was refined near the throat and along the walls to capture the steep acceleration.

Figure ?? shows the Mach-number and static-pressure contours; the symmetry-line distributions are in Fig. ???. The solution accelerates smoothly through $M \approx 1$ at the throat, reaches $M \approx 3$ in the diverging section, and exhibits no internal shocks, as desired for a minimum-length nozzle.

9.3 MOC–CFD comparison and validation

A quantitative cross-check between the MOC prediction (inviscid, isentropic) and the RANS solution (viscous, with boundary layer) shows very good agreement:

- **Exit Mach number.** Centerline CFD yields $M_e^{\text{CFD}} \approx 2.95\text{--}3.00$ (plateau in Fig. ??), within $\sim 2\%$ of the MOC target $M_e = 3.05$.
- **Exit static pressure.** The symmetry-line pressure approaches $\sim 2.7 \times 10^4$ Pa, i.e., $p_e/p_0 \approx 0.027$, within $\sim 7\%$ of the isentropic value 0.0253 in Table 1.
- **Shock-free interior.** No internal normal shocks are observed in the CFD contours; characteristics are effectively “straightened” by the minimum-length wall, matching the MOC design objective of parallel, uniform exit flow.

The small discrepancies are consistent with viscous effects (boundary-layer growth reduces the effective area ratio), turbulence modeling, and numerical diffusion, none of which are present in the MOC.

9.4 Uncertainty and limitations

The MOC assumes 2D, steady, inviscid, irrotational, and isentropic flow with constant γ . The CFD uses a RANS closure (SST) with a constant molecular viscosity and Prandtl model; wall heat transfer was set to zero. The present study did not include a grid-convergence index; however, the mesh was refined around the throat and along the wall to minimize resolution errors in the acceleration zone.

10 Conclusions

1. A *minimum-length* supersonic nozzle for $M_e = 3.05$ was designed via the Method of Characteristics. The resulting diverging length is $L_{\text{div}} \approx 2.013$ meter with a wall maximum turn $\theta_{w,\text{max}} = \nu(M_e)/2 = 12.678^\circ$.
2. The geometric outputs (wall locus and area ratio $A_e/A_t \approx 20.42$) and the complete set of nodal states were generated and tabulated.
3. Independent CFD (SU2, RANS–SST) confirmed the design: the flow accelerates smoothly to $M \approx 3$ without internal shocks; the centerline pressure ratio is within 7% of the isentropic prediction.
4. Differences between MOC and CFD are attributable to viscous effects, turbulence modeling, and outlet-backpressure control. No qualitative deviations (e.g., shocks or separation) were observed.

Practical takeaway. The MOC remains an efficient and reliable tool for first-cut shaping of high-speed nozzles. A short, minimum-length contour that enforces $\theta \rightarrow 0$ at the exit achieves a nearly uniform supersonic jet when coupled with a backpressure matched to the isentropic design. Subsequent CFD (and, if needed, grid-refinement studies and conjugate heat-transfer modeling) can be used to incorporate viscous corrections and manufacturing constraints.